



**A new metric for relating macroscopic chromatograms to  
microscopic surface dynamics: the Distribution Function  
Ratio (DFR)**

Journal:	<i>Analyst</i>
Manuscript ID	AN-ART-03-2021-000370.R1
Article Type:	Paper
Date Submitted by the Author:	12-May-2021
Complete List of Authors:	Bishop, Logan; Rice University, Chemistry Misiura, Anastasiia; Rice University, Chemistry Landes, Christy; Rice University, Chemistry

# A new metric for relating macroscopic chromatograms to microscopic surface dynamics: the Distribution Function Ratio (DFR)

Logan D.C. Bishop<sup>†</sup>, Anastasiia Misiura<sup>†</sup>, Christy F. Landes<sup>†‡§</sup> <sup>//</sup> \*

<sup>†</sup>Department of Chemistry, <sup>‡</sup>Department of Electrical and Computer Engineering, <sup>§</sup>Department of Chemical and Biomolecular Engineering, and <sup>//</sup> Smalley-Curl Institute, Rice University, Houston, Texas 77251, USA

\* Corresponding Author: [cflandes@rice.edu](mailto:cflandes@rice.edu)

## Abstract

Heterogeneous stationary phase chemistry causes chromatographic tailing that lowers separation efficiency and complicates optimizing mobile phase conditions. Model-free metrics are attractive for assessing optimal separation conditions due to the low quantity of information required, but often do not reveal underlying mechanisms that cause tailing, for example, heterogeneous retention modes. We report a new metric, which we call the Distribution Function Ratio (DFR), based on a graphical comparison between the chromatogram and Gaussian cumulative distribution functions, achieving correspondence to ground truth surface dynamics with a single chromatogram. Using a Monte Carlo framework, we show that the DFR can predict the prevalence of heterogeneous retention modes with high precision when the relative desorption rate between modes is known, as in during surface dynamics experiments. Ground truth comparisons reveal that the DFR outperforms both the asymmetry factor and skewness by yielding a one-to-one correspondence with heterogeneous retention mode prevalence over a broad range of experimentally realistic values. Perhaps of more value, we illustrate that the DFR, when combined with the asymmetry factor and skewness, can estimate microscopic surface dynamics, providing valuable insights into surface chemistry using existing chromatographic instrumentation. Connecting ensemble results to microscopic quantities through the lens of simulation establishes a new chemistry-driven route to measuring and advancing separations.

## 1. Introduction

Understanding the microscopic surface mechanisms underlying chromatographic separations is crucial for moving drug production from quality by testing<sup>1</sup> to quality by design.<sup>2</sup> Doing so

1  
2  
3 would help reduce the purification and separation cost of new protein pharmaceuticals as well as  
4 alleviate the energy burden induced by industrial separations.<sup>3-5</sup> Recent efforts to move towards  
5 separations-by-design include novel column designs, continuous flow systems, new single-analyte  
6 measurements, advanced statistical analysis, and mechanistic simulations and theory.<sup>1, 6-19</sup> It is thus  
7 possible to correlate microscopic phenomena to ensemble observables such as chromatographic  
8 elution curves. Most discussions of tailing address column overloading,<sup>20-22</sup> but tailing can also  
9 occur due to rare, heterogeneous interactions with the stationary phase surface. Surface  
10 heterogeneity can be introduced by surface defects<sup>7, 9</sup> or result from specific versus non-specific  
11 binding,<sup>12</sup> an effect often seen in chiral separations.<sup>23</sup> Ideally, we also need new methods to extract  
12 mechanistic details from macroscopic separations observables.

13  
14  
15  
16  
17  
18  
19  
20  
21  
22  
23  
24  
25  
26  
27 Detailed chemical information is captured in the lineshape of a chromatogram. Lineshape  
28 analysis can infer the number of adsorption events in the column,<sup>24</sup> varied adsorption kinetics,<sup>25</sup>  
29 non-linear column contributions,<sup>26</sup> and flow effects.<sup>27-28</sup> Other methods rely on analytical models  
30 that approximate the curve using variables without physical meaning,<sup>28-29</sup> fitting peaks based on  
31 analytical series,<sup>30</sup> or need ancillary equipment during data collection.<sup>31-32</sup> Conversely, model-less  
32 metrics using only the chromatogram have been utilized to interpret microscale phenomena and  
33 are common metrics for separation optimization<sup>33-34</sup> but rarely can relate changes in chromatogram  
34 shape to changes in stationary phase surface chemistry. Here, a disconnect forms between relating  
35 the results of an ensemble separation performed in a column measured in millimeters to  
36 microscopic details measured over micrometers of stationary phase surface, such as those captured  
37 in single-molecule studies.<sup>35-37</sup> Recently, we demonstrated that the most popular graphical metric,  
38 the asymmetry factor ( $A_s$ ), is not suitable for microscale studies of surfaces due to non-linear  
39 relationships with respect to rare retention mode statistics and underestimation of the amount of  
40  
41  
42  
43  
44  
45  
46  
47  
48  
49  
50  
51  
52  
53  
54  
55  
56  
57  
58  
59  
60

1  
2  
3 analyte lost in the tail.<sup>38</sup> Development of a graphical metric that infers surface chemical effects  
4  
5 from ensemble chromatograms would translate decades of opaque experimental optimization into  
6  
7 powerful observations of chemical phenomena occurring on the stationary phase surface.  
8  
9

10 The Distribution Function Method (DFM)<sup>39-41</sup> detects peak variations by comparing two  
11  
12 distributions in a parametric plot, providing qualitative proof of minute deviation, but lacking  
13  
14 correlation to an underlying mechanism. Repurposing the DFM to create trackable phenomena can  
15  
16 correlate chromatogram lineshape to ground truth physical chemistry at the surface like mixed-  
17  
18 mode adsorption<sup>42</sup> and stationary phase hopping<sup>43</sup> from ensemble data alone. Pivoting to include  
19  
20 mobile phase simulations could extend correlations to mobile phase artifacts from flow<sup>44-45</sup> and  
21  
22 column structure,<sup>46-50</sup> extra column components and injection methods,<sup>51-53</sup> and diffusion within  
23  
24 pores.<sup>54-57</sup> Using the paradigms of the DFM to produce trackable metric phenomena from a library  
25  
26 of simulated chromatograms creates a new quantitative metric sensitive to microscale  
27  
28 physicochemistry occurring in the column while only needing ensemble input. Correlation of  
29  
30 simulated effects with chromatogram lineshape provides a necessary bridge between macroscale  
31  
32 and microscale measurements.<sup>58-59</sup>  
33  
34  
35  
36  
37  
38

39 In this work, we expand the DFM as a ratio of the chromatographic cumulative distribution  
40  
41 function (CDF) and a Gaussian CDF, a method we call the Distribution Function Ratio (DFR), to  
42  
43 calculate microscopic surface dynamics from a single chromatogram. Comparisons to a Gaussian  
44  
45 lineshape improve upon Rix's original method by eliminating the need for ancillary peaks to  
46  
47 characterize the chromatogram.<sup>40</sup> Further, chromatogram lineshape is shown to correlate pseudo-  
48  
49 linearly to mixed-mode adsorption dynamics, capturing important surface statistics using only the  
50  
51 ensemble chromatogram. Mixed-mode adsorption dynamics, a model for kinetic tailing in low  
52  
53 dilution and topic of interest for pharmaceutical separations,<sup>60-61</sup> are used to simulate  
54  
55  
56  
57  
58  
59  
60

1  
2  
3 chromatograms from ground truth statistics and demonstrate the utility and precision of the DFR.  
4  
5 Here, we show that the DFR outperforms  $A_s$  and statistical skewness over a wide range of relative  
6  
7 prevalence and relative desorption rate of rare, high energy, slow desorbing retention modes on  
8  
9 the stationary phase surface. Use of the DFR with microscale surface information provides high  
10  
11 precision estimates of surface retention modes. However, in absence of microscale surface insight,  
12  
13  $A_s$  and skewness can be used in combination with the DFR to estimate surface dynamics from the  
14  
15 ensemble peak alone. The DFR is used to analyze a separation of a model protein, lysozyme,  
16  
17 capturing valuable statistics about surface retention modes. Combining the DFR with ground truth  
18  
19 simulations generates calibration curves that connect peak shape to surface physicochemistry,  
20  
21 creating an optimizable metric that interrogates stationary phase surface dynamics while reporting  
22  
23 on the quality of separation. Using the DFR quantifies rare surface defects and specific adsorption  
24  
25 using only ensemble chromatography.  
26  
27  
28  
29  
30

## 31 **2. Experimental Section**

### 32 **2.1 Theory**

33  
34  
35 Tracing the source of mixed-mode kinetic tailing requires knowledge of the prevalence and  
36  
37 desorption statistics of retention modes on the stationary phase surface. We examine tailing in  
38  
39 mixed-mode chromatography where a protein alternates between flowing in the mobile phase and  
40  
41 surface adsorption through two different retention modes, the first mode fast desorbing and  
42  
43 prevalent, the other slower desorbing and increasingly rare. Each retention mode has a distinct rate  
44  
45 of desorption ( $k_j$ ) and expected desorption time ( $\langle\tau_j\rangle$ ) that describes an exponential distribution of  
46  
47 singular desorption times ( $\tau_j$ ), where higher energy retention modes have longer expected  
48  
49 desorption times.<sup>62</sup> Stationary phases with two retention modes ( $m = 2$ ) induce tailing and  
50  
51  
52  
53  
54  
55  
56  
57  
58  
59  
60

1  
2  
3 broadening in chromatography,<sup>61, 63-64</sup> though a proliferation of retention modes ( $m > 2$ ) can exist  
4  
5 depending on surface microstructure and functionalization.<sup>65-68</sup> The number of retention modes on  
6  
7 the surface and their desorption rates can be gathered experimentally using microscale, surface  
8  
9 measurements.<sup>11, 13</sup> However, direct observations of surface dynamics are limited spatially, on the  
10  
11 order of micrometers, while column lengths are on the millimeter scale. Capturing the desorption  
12  
13 time differences between common and rare modes and correlating their prevalence to column-  
14  
15 wide experimental parameters is critical for reducing chromatographic tailing and can only be  
16  
17 achieved through simulation and theory.  
18  
19  
20  
21

22 Modeling the tailing effects of mixed-mode adsorption requires knowledge of molecular  
23  
24 elution histories. Kinetic chromatographic tailing occurs when a small population of molecules  
25  
26 forms a broad distribution of elution times due to interactions with a rare, high energy retention  
27  
28 mode, even in dilute conditions where column overload does not occur.<sup>25, 64</sup> The stochastic theory  
29  
30 of chromatography captures rare interactions by describing molecular elution as a molecule  
31  
32 undergoing a random walk between moments of mobility and stationarity. The elution history of  
33  
34 each molecule is then a series of connected adsorption events sampled from available retention  
35  
36 modes.<sup>69</sup> A master equation for the retention time of a single molecule ( $T$ ) that incorporates  
37  
38 interactions for every adsorption event across all retention modes is then **Equation 1**:  
39  
40  
41  
42  
43

$$44 \quad T = t_m + t_s = t_m + \sum_{j=1}^m \sum_{i=1}^n \tau_{i,j} \quad (1)$$

45 where  $t_m$ ,  $t_s$  represent the sums of time spent in the mobile, stationary phase and  $\tau_{i,j}$  is the length  
46  
47 of time spent during the  $i^{\text{th}}$  adsorption event through the  $j^{\text{th}}$  retention mode.<sup>70</sup> Here, assumption of  
48  
49 a constant mobile phase time ( $t_m$ ) isolates the tailing contribution of heterogeneous adsorption  
50  
51 rather than convolve it with mobile phase effects, of which there are many.<sup>71-72</sup> A chromatogram  
52  
53  
54  
55  
56  
57  
58  
59  
60

1  
2  
3 can be simulated by aggregating thousands of results from **Equation 1** using Monte Carlo methods  
4  
5 educated by ground truth chemical quantities found in surface studies, correlating retention mode  
6  
7 energy/prevalence to different tailing metrics.<sup>73</sup>  
8  
9

10  
11 The molecular histories produced by the Monte Carlo simulations are random samples of the  
12  
13 “frequency functions” described by Dondi.<sup>74-75</sup> Analytically, each frequency function is the sum  
14  
15 of all  $n^{\text{th}}$  fold convolutions of the distribution of the retention mode desorption times over  $n$   
16  
17 adsorption/desorption steps for  $0 \leq n \leq \infty$ . For the homogeneous case, the stationary phase time,  
18  
19  $c_s(t)$ :  
20  
21

$$22 \quad c_s(t) = \sum_n P(n) f_{s,1}(\tau)^{n*} \quad (2)$$

23  
24 where  $P(n)$  is the probability of a molecule undergoing  $n$  adsorption/desorption steps,  $f_{s,1}(\tau)$  is  
25  
26 the distribution of desorption times for the common mode, and  $n^*$  is the  $n^{\text{th}}$  fold convolution. For  
27  
28 the heterogeneous two-retention mode case, the equation can be expanded to **Equation 3** for  
29  
30  $0 \leq n \leq \infty$ , per Cavazzini.<sup>61</sup>  
31  
32  
33  
34  
35

$$36 \quad c_s(t) = \sum_n P(n) f_{s,1}(\tau)^{n*} + \sum_n P(n) \sum_{j=0}^{n-1} \binom{n}{j} p^j (1-p)^{n-j} f_{s,1}^{j*}(\tau) * f_{s,2}^{(n-j)*}(\tau) \quad (3)$$

37  
38 where  $\binom{n}{j} p^j (1-p)^{n-j}$  is the Bernoulli coefficient for  $j$  interactions with the common retention  
39  
40 mode with relative prevalence  $p$  out of  $n$  total adsorption/desorption steps and  $f_{s,2}(\tau)$  is the  
41  
42 distribution of desorption times for the rare retention mode. Monte Carlo simulations avoid  
43  
44 convolutions by directly calculating the sum of random variables over  $n$  adsorption/desorption  
45  
46 steps, constructing the distributions in  $c_s(t)$  through random sampling. As such, we define  $c_s(t)$   
47  
48 non-analytically as a mixture model<sup>76</sup> of our Monte Carlo calculated molecular history  
49  
50  
51  
52  
53  
54  
55  
56  
57  
58  
59  
60

distributions where each distribution is differentiated by the number of interactions with a rare retention mode (**Equation 4**):

$$c_s(t) = \alpha_1 f_1(t) + \alpha_2 f_2(t) + \sum_{i=3}^m \alpha_i f_i(t) \quad (4)$$

Where  $f_i(t)$  are the distributions of molecular retention times that have interacted with the  $i^{\text{th}}$  rare retention mode and  $\alpha_i$  represent the fraction of molecular histories sampled from the  $i^{\text{th}}$  subpopulation and must sum to 1. Here,  $f_1(t)$  describes the homogenous distribution of molecular histories, equivalent to **Equation 2**, and  $f_2(t)$  is equivalent to the second term in **Equation 3**. The third term of **Equation 4** includes any additional modes past the first rare mode. In transitioning from **Equation 3** to **Equation 4**, we have released the requirement that  $n$  be strictly known in favor of functions that can be analyzed by profile shape. The visual result of **Equation 4** is presented in **Figure S1**. To utilize **Equation 4** in our analysis, we have assumed that the mobile phase contribution has been removed by deconvolution with the distribution of an unretained tracer analyte.<sup>24, 80</sup> Contributions to  $t_m$  include flow heterogeneity due to stationary phase structural imperfections and extra-column factors, both leading to asymmetry or broadening.<sup>77-79</sup> The long column approximation guarantees that the homogeneous population forms a Gaussian ( $f_1(t) \approx g(t)$ ) when a sufficient number of adsorption events have occurred and is often considered the ideal peak shape.<sup>15, 34</sup> However, achieving the Gaussian limit when heterogeneous adsorption is present requires columns not usually seen in practice.<sup>81</sup> Several studies have shown that comparisons to a Gaussian can quantify asymmetry of the lineshape<sup>82-83</sup> or estimate sub-resolution curves when proper assumptions are made.<sup>84</sup> Combining **Equation 4** and the long column approximation establishes that any deviations from the Gaussian lineshape carry information about the tailing distributions  $\sum_i^m f_i(t)$ . Quantifying deviations from the Gaussian distribution is then an avenue to



1  
2  
3 measure statistics of the tailing distributions in the chromatogram lineshape without specifying an  
4 analytical model for each distribution  $f_i(t)$ .  
5  
6  
7

## 8 **2.2 Metric Definition**

9

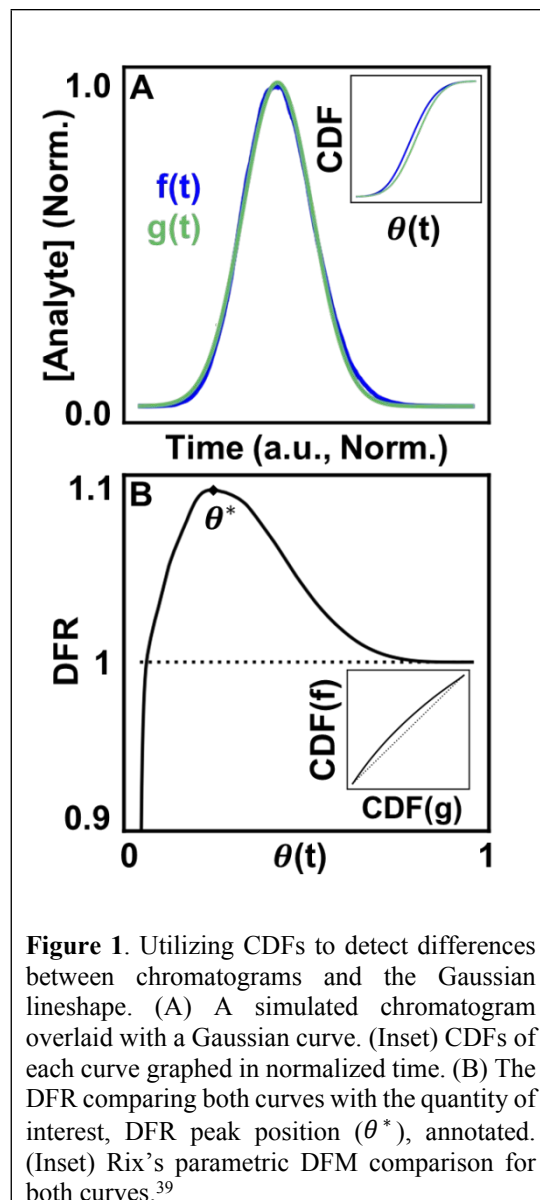
10  
11 Methods developed from the DFM<sup>39-40</sup> can detect small deviations in the lineshape of two  
12 distributions while remaining tolerant to excessive experimental noise.<sup>39</sup> Briefly, the DFM  
13 qualitatively differentiates two distributions (**Figure 1A**) by comparing the shape of each  
14 chromatogram's CDF (**Figure 1A, inset**) normalized to the time interval (0,1] through the function  
15  $\theta(t)$  (see SI), and abbreviated as  $\theta$  when used as a variable. Our modification of the DFM always  
16 compares to a Gaussian CDF, adopting the Gaussian as the 'ideal' chromatogram through the  
17 posing of **Equation 4**. Further, taking the ratio of both CDFs generates trackable peak phenomena,  
18 providing quantitative tracking of underlying physical chemistry rather than qualitative  
19 acknowledgment of the difference of two chromatograms, as in Rix's original work.  
20  
21 Mathematically, the DFR for any chromatogram/Gaussian pair ( $c(\theta), g(\theta)$ ) is then the ratio of their  
22 CDFs (see SI) over the normalized time interval  $\theta$  (**Equation 5**):  
23  
24  
25  
26  
27  
28  
29  
30  
31  
32  
33  
34  
35  
36  
37

$$38 \text{DFR}(0 < \theta \leq 1; c(\theta), g(\theta)) = \frac{\int_0^\theta c(t) dt}{\int_0^\theta g(t) dt} = \frac{C(\theta)}{G(\theta)} \quad (5)$$

39  
40  
41  
42  
43  
44  
45  
46  
47  
48  
49  
50  
51  
52  
53  
54  
55  
56  
57  
58  
59  
60

1  
2  
3  
4  
5  
6  
7  
8  
9  
10  
11  
12  
13  
14  
15  
16  
17  
18  
19  
20  
21  
22  
23  
24  
25  
26  
27  
28  
29  
30  
31  
32  
33  
34  
35  
36  
37  
38  
39  
40  
41

The result of **Equation 5** is a unique, characteristic curve for every chromatogram (**Figure 1B**) with a critical value in the form of peak position ( $\theta^*$ ). Generating quantitative, optimizable peak phenomena differentiates the DFR from the original DFM result (**Figure 1B, inset**), which only qualitatively assesses if two distributions are different through deviations along the diagonal. As such, two separate chromatograms are needed to quantify chemical effects in a single experiment. The DFR retains the benefits of Rix's original method in only utilizing the chromatogram lineshape without fitting to a model but extracts chemical information through comparison to the Gaussian curve normalized in time and concentration, avoiding the need for a second chromatogram. Normalization also minimizes the contribution of broadening by the mobile phase



42  
43  
44  
45  
46  
47  
48  
49  
50  
51  
52  
53  
54  
55  
56  
57  
58  
59  
60

(**Figure S2**), further isolating the stationary phase contributions. Because deviations from a Gaussian represent contributions due to heterogeneous surface interactions, per **Equation 4**, information about the tailing distributions is captured in the DFR lineshape. Ground truth simulations correlate the energy and prevalence of rare retention modes to the chromatogram lineshape and validate that the DFR can capture statistics of tailing distributions. The DFR provides an estimate of the relative column prevalence of a retention mode identified through

1  
2  
3 microscale surface measurements, bridging the spatial difference between surface dynamics  
4 measurements ( $\mu\text{m}$  scale) and the full-length column (mm scale). Further, estimating microscopic  
5 surface dynamics from the ensemble chromatogram alone provides a no-cost evaluation of the  
6 need for more complex, micrometer resolution experiments.  
7  
8  
9  
10  
11  
12

### 13 **2.3 Computational Details**

14  
15  
16 Chromatographic simulations were performed using a Monte Carlo framework programmed  
17 in Python 3 programming language<sup>85</sup> (Python Software Foundation, <https://www.python.org/>)  
18 using Numpy<sup>86</sup> and Scipy.<sup>87</sup> The simulation framework is based on the work of Dondi<sup>15</sup> and  
19 Cavazinni,<sup>14</sup> and detailed in our previous publications.<sup>11, 38</sup> The benefits of the Monte Carlo  
20 framework is that it is agnostic towards retention mechanisms when the mathematics are properly  
21 posed and is the only route for modeling non-linear chromatography.<sup>88-89</sup> Surface crowding is not  
22 included in the simulations, meaning that all chromatographic artifacts are the product of kinetic  
23 tailing rather than thermodynamic column overloading. Therefore, changes measured with the  
24 DFR only relate to surface kinetic effects, a connection unachievable experimentally and only  
25 partially realized in microscale surface experiments without simulation. The simulations treat time  
26 and distance as abstract, unitless quantities that are adaptable to any column length or surface  
27 chemistry. Time is measured in the unitless value  $\delta t$ , which adapts to the units of the kinetic rate  
28 for the retention mode.<sup>90</sup> Our Monte Carlo simulation framework treats each molecular elution as  
29 a random walk down a connected series of column ‘slices’, where the slice width is the expected  
30 travel distance between transitions in the mobile-stationary phase interface. Elution speed is set  
31 such that each molecule takes 1  $\delta t$  to traverse a column slice. For the simulations in this work, the  
32 simulated column has 1000 column slices with a constant mobile phase time  $t_m = 1000 \delta t$ . The  
33  
34  
35  
36  
37  
38  
39  
40  
41  
42  
43  
44  
45  
46  
47  
48  
49  
50  
51  
52  
53  
54  
55  
56  
57  
58  
59  
60

number of slices correlates to the difference in linear distance between a wide-field microscope field of view ( $\sim 32 \mu\text{m}$ ) and a real column ( $\sim 30 \text{mm}$ ).

Adsorption events are simulated using statistical sampling parameterized by the probability of interaction with the stationary phase surface, the probability of encountering a specific retention mode ( $p_j$ ), and the expected desorption time of that retention mode ( $\langle \tau_j \rangle$ ). A schematic for the random walk a molecule undergoes in each slice is shown in **Figure 2**. Here, we assume each molecule has a probability ( $p_a = 0.5$ ) of undergoing adsorption exactly

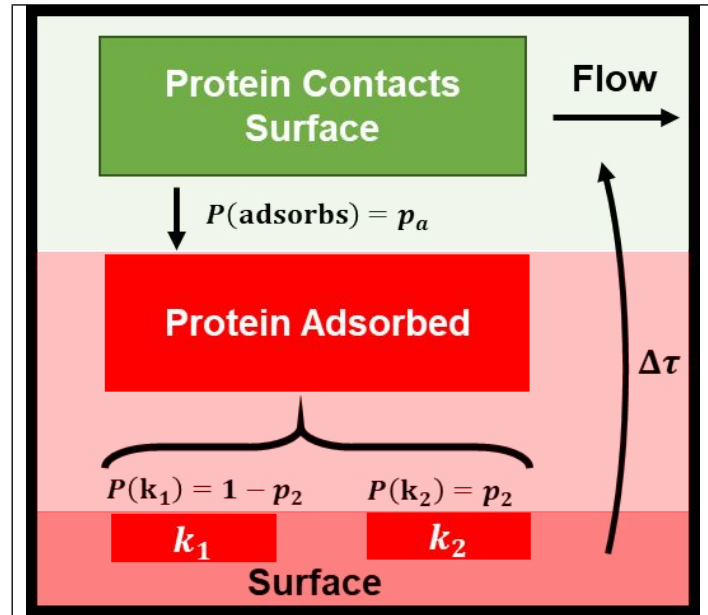


**Figure 2.** A graphical depiction of a simulated column ‘slice’ showing the probabilistic decision branches to simulate interactions with the stationary phase. A protein encounters the surface, undergoes adsorption with some probability ( $p_a$ ), and adsorbs to the surface through one of  $j$  retention modes with a likelihood of selection  $p_j$ . Figure modified with permission from ref. 32. Copyright Elsevier 2020.

once within each slice. The probability of interaction with the surface is arbitrarily chosen but operates as a tunable parameter adjusted to fit available surface dynamics data. The original stochastic theory assumes that an average probability is satisfactory if a molecule fluctuates through the range of adsorption probabilities many times between adsorptions.<sup>69</sup> Further, Hlushkou et al. have described the probability of adsorption upon interaction with the surface as a constant based upon geometrical and energetic consideration for the adsorption process.<sup>90-91</sup> However, we note that our probability is conditioned on the phase ratio of the column and could be expanded to include local heterogeneity of the stationary phase surface. Including local fluctuations in

1  
2  
3 probability in the model framework is a natural extension as more experimental information  
4  
5 becomes available.  
6  
7

8 Each slice can be considered a column feature, such as a bead, similar to the description  
9 provided by Horvath *et al.*<sup>92</sup> The ‘surface’ of each slice has  $m$  retention modes, each with some  
10 probability of selection ( $p_j$ ). In the case of our simulations, the probability of interacting with the  
11 low energy, faster desorbing retention mode is higher than interaction with high energy, slower  
12 desorbing retention mode ( $p_1 \gg p_2$ ). After retention mode selection, a desorption time ( $\Delta\tau$ ) is  
13 sampled from an exponential distribution parameterized on the desorption rate constant of the  
14 retention mode ( $e^{-\tau k_j}$ ) with expected desorption time of  $\langle\tau_j\rangle = \frac{1}{k_j}$ .<sup>24,62</sup> Simulating many molecules  
15 down the column and aggregating the elution histories together generates a chromatogram.  
16  
17  
18  
19  
20  
21  
22  
23  
24  
25  
26  
27

## 28 **2.4 Experimental methods**

29  
30

31 The chromatographic experiments were carried out using a home-built Fast Protein Liquid  
32 Chromatography (FPLC) system. Protein solutions of 8.3  $\mu\text{M}$  Lysozyme from chicken egg white  
33 (>98%; Sigma) in the presence of 1M sodium chloride (NaCl) were prepared in 10 mM HEPES  
34 buffer (Sigma, pH 7.2). All the solutions were injected into the FPLC using a 1 mL syringe  
35 (Becton Dickinson) with an injection volume of 300 $\mu\text{L}$ . A constant flow of 2 ml/min was  
36 controlled using a peristaltic pump (Watson-Marlow, 120 Series). Absorbance from the analyte  
37 was monitored at 280 nm using a UV detector (Spectrum Chromatography). The signal then was  
38 converted from current to voltage by a digital recorder (Hantek, 365E) controlled by Hantek 365  
39 software that registered the output signal. The syringe hydrophilic filters with polyvinylidene  
40 fluoride (PVDF) membranes (hydrophilic 0.45  $\mu\text{m}$  pore size, 25 mm diameter) and hydrophobic  
41 filters with PVDF membranes (hydrophobic 0.45  $\mu\text{m}$  pore size, 25 mm diameter) used as  
42  
43  
44  
45  
46  
47  
48  
49  
50  
51  
52  
53  
54  
55  
56  
57  
58  
59  
60

1  
2  
3 chromatographic media were purchased from Cole-Parmer and Sigma Aldrich, respectively. A  
4 series of three connected PVDF syringe filters were assembled and integrated with the setup. All  
5 components of the FPLC system were connected using silicone tubing (MED-X.D., 0.063" internal  
6 diameter).  
7  
8  
9  
10  
11  
12

## 13 2.5 Computational Details

14  
15

16 A two-mode system was simulated using four different ratios of desorption rates over a range  
17 of strong retention mode prevalence. The common, low energy retention mode has an expected  
18 desorption time of  $\langle \tau_1 \rangle = 4 \delta t$ , equivalent to four times as long as necessary to traverse the column  
19 slice. Expected desorption times of the rare, high energy retention mode are then a factor longer  
20 than the expected desorption times of the common, low energy retention mode ( $\frac{\langle \tau_2 \rangle}{\langle \tau_1 \rangle} = 5, 25, 50$   
21 , 125) over a range of relative prevalence ( $10^{-5} \leq p_2 \leq 10^{-2}$ ) covering several orders of  
22 magnitude. Relative prevalence is defined with respect to the number of slices in the column. Here,  
23 the relative prevalence relates to the absolute number of times a molecule interacts with a rare site  
24 ( $0.01 \leq \langle j_{m=2} \rangle \leq 10$ ). Each simulation consisted of 300,000 simulated molecules, which was  
25 shown to be sufficient for stabilization of the curve shape (**Figure S3**). The distribution of  
26 adsorption events per molecule ( $n$ ) forms a Gaussian about  $\langle n \rangle = 500$  given a 50% chance of  
27 adsorbing to the surface in a 1000 slice column. The average number of adsorption-desorption  
28 events as well as the chance of adsorbing to the stationary phase can be validated through peak  
29 analysis of ensemble data.<sup>14, 24</sup> Adjusting the probability of adsorption ( $p_a$ ) and the number of  
30 slices will change the value of  $n$  and therefore the shape of the chromatogram. However, previous  
31 studies with similar theories and models have extracted useful information from a small number  
32 of interactions and discussed methods for scaling the profile in terms of the average number of  
33  
34  
35  
36  
37  
38  
39  
40  
41  
42  
43  
44  
45  
46  
47  
48  
49  
50  
51  
52  
53  
54  
55  
56  
57  
58  
59  
60

1  
2  
3 adsorption events.<sup>14-15, 74, 93</sup> Simulated molecule histograms are smoothed with a Savitzky-Golay  
4 filter before cubic splining, producing the final chromatographic curve used for analysis (**Figure**  
5  
6 **S4**).<sup>94-95</sup>  
7  
8  
9

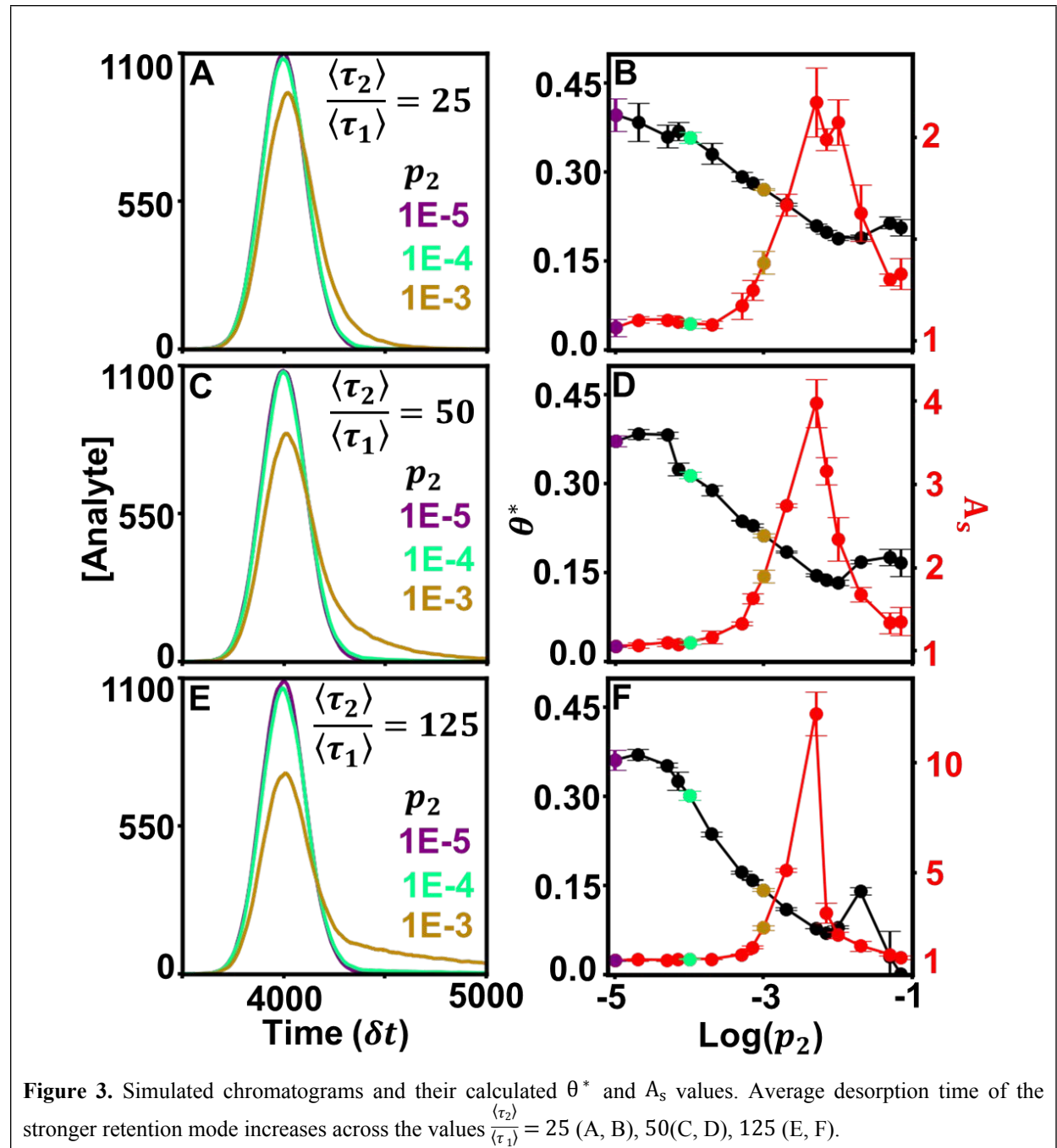
10 Functions that are used in the DFR must be normalized in time and concentration. The time  
11 domain is normalized using the function  $\theta(t)$  beginning/ending when the signal passes  
12 above/below a defined percent of the peak height. The recovered mass within those bounds is  
13 normalized to one ( $\int c_s(\theta(t))dt = 1$ ). The bounds chosen for each sample are 1% of the max  
14 height of  $c_s(t)$ . The shape of  $c_s(t)$  is compared to a Gaussian distribution in  $\theta$  with the mean at  $\theta$   
15 = 0.5. Normalization of time and mass generates the same Gaussian curve for any chromatographic  
16 peak making any form of peak fitting unnecessary. Bounds for the Gaussian CDF ( $G(\theta) =$   
17  $\int g(\theta)d\theta$ ) is set to 1.5% the max height of the representative Gaussian. How bound selection  
18 changes the shape of  $G(\theta)$  (**Figure S5A**) and the percent of the curve that falls outside the bounds  
19 (**Figure S5B**) are shown in the SI. DFR peak position ( $\theta^*$ ) is found using the first derivative test.  
20  
21  
22  
23  
24  
25  
26  
27  
28  
29  
30  
31  
32  
33

#### 34 **4. Results and Discussion**

35  
36  
37  
38  
39  
40  
41  
42  
43  
44  
45  
46  
47  
48  
49  
50  
51  
52  
53  
54  
55  
56  
57  
58  
59  
60

#### 4.1 Extracting relative desorption rate and high energy retention mode prevalence using the DFR.

Curvature changes in the chromatographic lineshape encode information about the relative prevalence of stronger retention modes at the stationary phase surface and are extractable by



tracking the DFR peak position ( $\theta^*$ ). **Figure 3** compares the sensitivity of  $\theta^*$  and  $A_s$  to changes



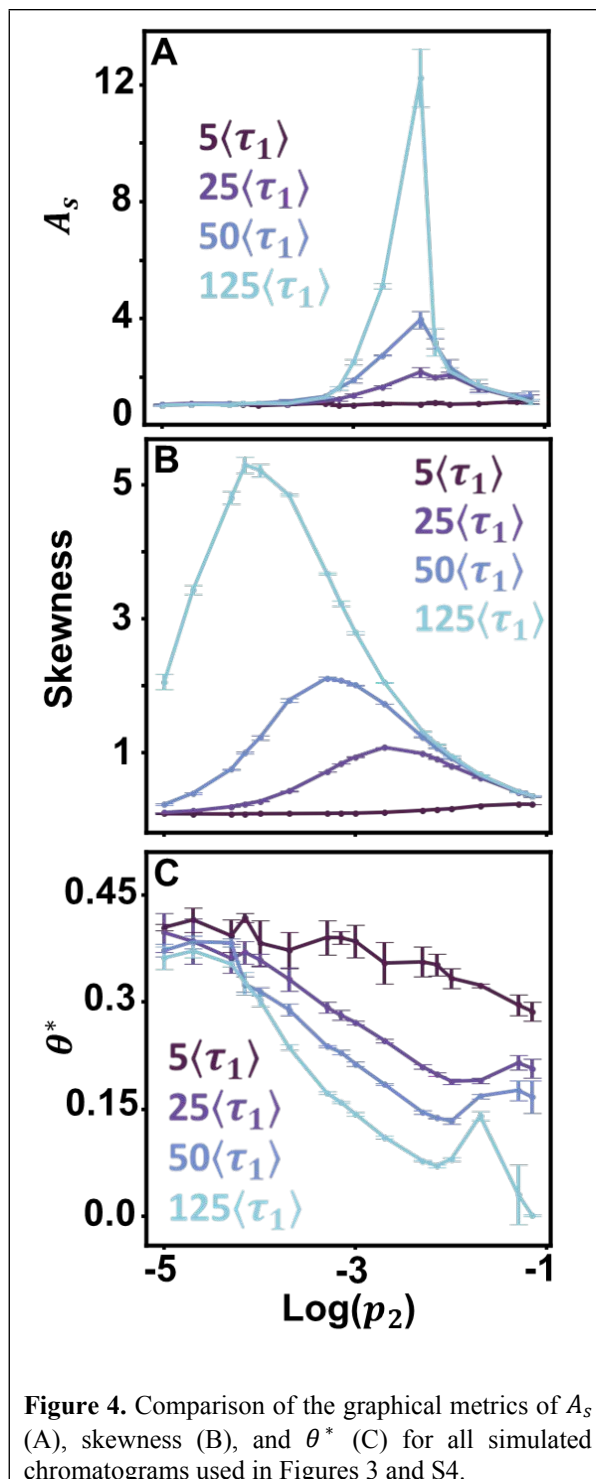
1  
2  
3 in the prevalence of the high energy retention mode ( $p_2$ ) at several relative desorption rates  $\left(\frac{\langle\tau_2\rangle}{\langle\tau_1\rangle}\right)$   
4  
5 = 25, 50, 125). At minor differences in desorption rates, low enough that chromatographic peaks  
6  
7 are visually similar (**Figure 3A**),  $\theta^*$  still detects surface heterogeneity at low levels of prevalence  
8  
9 and can differentiate between prevalence with high precision (**Figure 3B**).  $A_s$  does not share the  
10  
11 traits of sensitivity or differentiability, reporting homogeneity at low prevalence and losing  
12  
13 predictive power through lack of one-to-one correspondence at higher prevalence. Higher  
14  
15 desorption rate ratios  $\left(\frac{\langle\tau_2\rangle}{\langle\tau_1\rangle}\right)$  of 50 (**Figure 3C/D**) and 125 (**Figure 3E/F**) do not diminish the  
16  
17 precision or differentiability of the DFR or improve the results of  $A_s$ . Using  $A_s$  cannot provide an  
18  
19 accurate assessment of surface homogeneity, even when chromatograms visually tail. Tracking  $\theta^*$   
20  
21 provides a pseudo-linear, one-to-one correspondence over a wide range of prevalence with high  
22  
23 precision at a variety of different retention mode energies with a single chromatogram when the  
24  
25 ratio of desorption rates is known.  
26  
27  
28  
29  
30  
31  
32

33  
34 The DFR can still differentiate surface effects when the difference between retention mode  
35  
36 desorption rates nears homogeneity. **Figure S6** examines a kinetic scenario where the ratio of  
37  
38 expected desorption times between the low and high energy retention modes is a factor of 5. Small  
39  
40 differences in kinetics produce chromatograms that appear symmetric and are indifferentiable by  
41  
42 eye (**Figure S6A**).  $\theta^*$  tracks the prevalence of the slow retention mode while  $A_s$  is incapable of  
43  
44 differentiating between the peaks (**Figure S6B**). Development of custom-designed columns and  
45  
46 stationary phases<sup>96-97</sup> could be advanced by a metric that can interrogate surface heterogeneity at  
47  
48 a wide range of experimental conditions, especially near-homogeneous conditions that  
49  
50 approximate, but do not reach, the ideal Gaussian lineshape. Implementing the DFR in tandem  
51  
52  
53  
54  
55  
56  
57  
58  
59  
60

with surface dynamics measurements to direct the selection of macroscopic experimental parameters achieves chemistry-driven design of stationary phases.

#### 4.2 Tracking $\theta^*$ identifies surface dynamics when other graphical metrics fail.

Values of  $\theta^*$  are unique for each prevalence within a desorption rate trendline but are not unique between relative desorption rates. **Figure 4** graphs all four simulated chromatogram sets for three metrics:  $A_s$  (**Figure 4A**), skewness (**Figure 4B**), and  $\theta^*$  (**Figure 4C**). Identifying surface dynamics from the ensemble measurement requires a one-to-one correspondence trend across a wide range of possible prevalence values for the relative desorption rate. Here, both  $A_s$  and skewness either lose sensitivity over a range of values or provide two possible prevalence even when the relative desorption rate between modes is known. Knowledge of the surface dynamics



does not provide the means to correctly assess the prevalence of a retention mode in the full column. Conversely,  $\theta^*$  provides a near one-to-one correspondence over several orders of magnitude, providing an optimizable metric when the relative desorption rate

has been measured. Therefore, spatially limited microscale measurements of surface dynamics can extrapolate the rare retention mode prevalence across the length of the macroscale column. Complications arise when the relative desorption rates ( $\langle\tau_1\rangle, \langle\tau_2\rangle$ ) are unavailable to direct selection of a  $\theta^*$  trend line, such as when surface dynamics measurements have not been performed. Here, the one-to-one correspondence of  $\theta^*$  no longer holds when other relative desorption rates are considered (Figure 4C). Microscopy measurements are necessary to achieve a high precision estimate of surface dynamics, either in identifying relative desorption rate or relative prevalence of retention modes. However, aggregating several ensemble accessible metrics can educate the selection of relative desorption rate and mode prevalence.

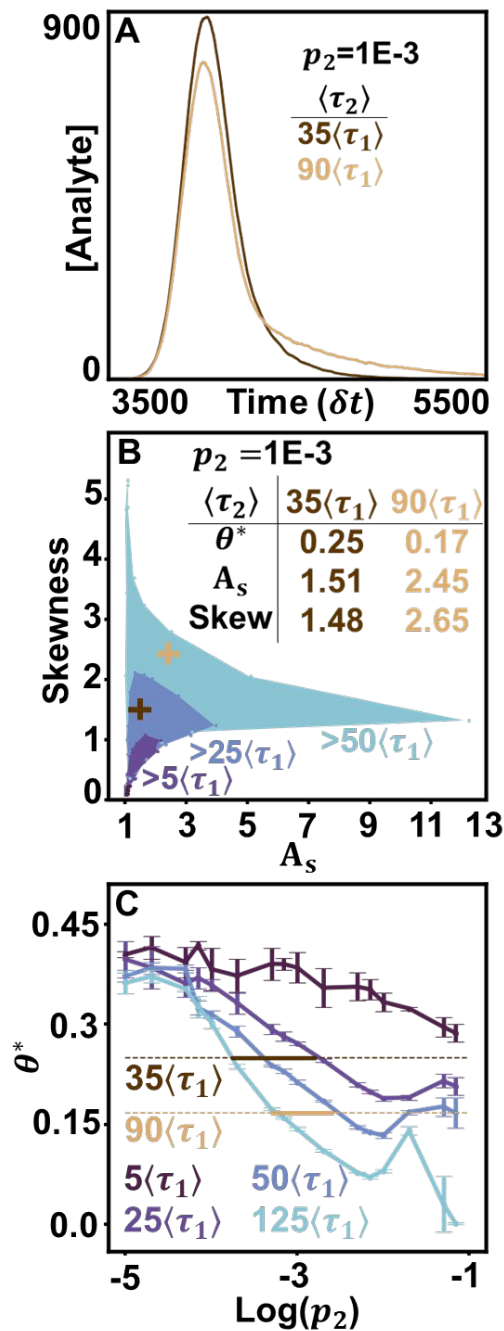


**Figure 5.** Estimating surface heterogeneity from ensemble information. (A) Simulated chromatograms with kinetic rates  $\frac{\langle\tau_2\rangle}{\langle\tau_1\rangle} = 35$  and  $95$  with  $p_2 = 0.001$ . (B) A parametric plot of  $A_s$  and skewness from Figure 4C trendlines. Chromatograms in panel A are denoted with crosses (C) All  $\theta^*$  trends with possible (dotted) and estimated (solid) solutions for simulated chromatograms from A.

### 4.3 Estimating mixed-mode prevalence and desorption rate without surface dynamics measurements.

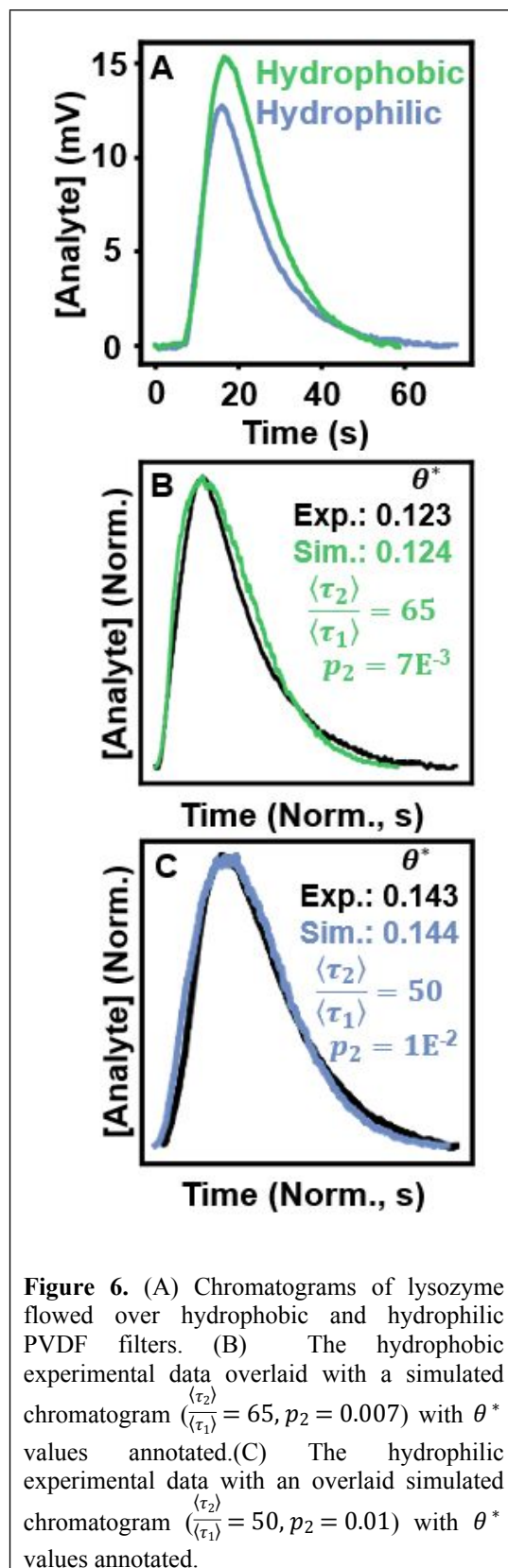
Combining  $\theta^*$  with ancillary graphical metrics can estimate  $p_2$  or  $\langle\tau_2\rangle$  when information about surface dynamics is unavailable. **Figure 5** presents a workflow for estimating surface heterogeneity from ensemble information alone. As an example, we consider two chromatograms with kinetics that do not lie along trendlines presented previously (**Figure 5A**). To direct selection of a  $\theta^*$  trendline, other graphical information can be incorporated. **Figure 5B** is a parametric plot of  $A_s$  versus skewness that can be used in the same manner as a phase diagram. Calculating both  $A_s$  and skewness can help estimate the value of  $\langle\tau_2\rangle$  from simulated data by identifying a range of valid relative desorption ratios. The values for the chromatograms in **Figure 5A** are marked with crosses and correctly estimate the relative desorption rate between retention modes for both simulations. **Figure 5C** illustrates possible solutions for  $\langle\tau_2\rangle$  and  $p_2$  for the simulated chromatograms given the values of  $\theta^*$ . Using information provided by the parametric plot in **Figure 5B**, the set of possible solutions (dotted line, **Figure 5C**) is reduced to a smaller estimate set with stricter bounds (solid line, **Figure 5C**). Here, we have successfully estimated the microscale surface values of  $\langle\tau_2\rangle$  and  $p_2$  from the ensemble chromatogram alone, bridging the knowledge gap through simulations.

### 4.4 Using $\theta^*$ to guide assessment of experimental chromatograms

Evaluating  $\theta^*$  in ensemble separations connect experimental results to simulated chromatograms, enabling analysis of plausible surface chemistry. The effectiveness of profile shape analysis has been illustrated experimentally using a library of standard control curves.<sup>98</sup> Here, we replicate that process using simulated two-retention mode curves to estimate surface dynamics in two

ensemble separations. **Figure 6** shows two real separations of lysozyme over hydrophobic and hydrophilic PVDF membranes and DFR analysis used to detect possible heterogeneity on the stationary phase surface. **Figure 6A** overlays the chromatograms for lysozyme flowed over hydrophobic and hydrophilic membranes. We begin our analysis with the assumption that the chromatogram can be best explained using a two-retention mode system, a kinetic scenario well studied in theory and commonly seen experimentally on otherwise homogeneous surfaces.<sup>9, 62, 66, 93, 99-100</sup> Subsequent, rarer, stronger retention modes are possible but negligibly contribute to profile shape (**Figures S1**).

**Figure 6B/C** present DFR analysis for the hydrophobic and hydrophilic separation, respectively, overlaying the experimental data with a simulated chromatogram that matches in  $\theta^*$ . In both cases, a simulated peak was found that showed good agreement with the raw data. Peak position/height were matched to reduce differences in  $t_m$  and normalize for concentration, respectively. The time-domain was normalized to account for differences



1  
2  
3 between the time resolution of the FPLC detector (0.6 ms) versus the simulated unit of time ( $\delta t$ ).<sup>89</sup>  
4  
5 Possible solutions for the surface kinetics are extrapolated from simulated chromatograms that  
6  
7 closely match the experimental curve shape and the experimental value of  $\theta^*$  (**Table S1** and **S2**).  
8  
9  
10 The subset of the simulations used to extrapolate the surface kinetics are co-plotted with the  
11  
12 experimental data in **Figures S7** and **S8**.  
13  
14

15 The matching simulated chromatograms indicate that the surfaces could be described using a  
16  
17 two-retention mode system where the rare, long binding mode has a relative desorption time of  $\frac{\langle \tau_2 \rangle}{\langle \tau_1 \rangle}$   
18  
19 = 65 and relative prevalence  $p_2 = 0.007$  on the hydrophobic membrane and  $\frac{\langle \tau_2 \rangle}{\langle \tau_1 \rangle} = 50$  and  $p_2$   
20  
21 = 0.01 on the hydrophilic membrane. Previous work in the group suggests that the transition from  
22  
23 hydrophobic to hydrophilic character decreases the hopping behavior of lysozyme on the  
24  
25 stationary phase surface.<sup>101</sup> Increased hopping motion, also called continuous-time random walks,  
26  
27 can lead to changes in peak shape.<sup>11</sup> The increase in the prevalence of long interactions on the  
28  
29 hydrophilic membrane could be caused by the increased unfolding of lysozyme on the hydrophilic  
30  
31 surface, where the change in surface character introduces a new mode of interaction.<sup>102</sup> Both  
32  
33 possibilities represent starting points for imaging of the stationary phase surface to understand the  
34  
35 possible chemical moieties that lead to rare surface interactions.  
36  
37  
38  
39  
40  
41  
42

43 Peak analysis of the hydrophilic surface homogeneous population was performed by removing  
44  
45 the contribution of interactions with the rare retention mode, a benefit of using simulations. Using  
46  
47 methods described by Felinger<sup>24</sup>, we estimate that  $\langle \tau_1 \rangle = 40$  ms if  $\langle n \rangle = 645$  (**Figure S9**). Both  
48  
49 values could be scaled to adjust for varied values of  $\langle n \rangle$ . We can conclude that  $\theta^*$  would be  
50  
51 suitable as a guide for automatically matching experimental chromatograms to simulated data as  
52  
53 the analysis only relies on the profile shape, not the chemical identity of the separatory mode or  
54  
55  
56  
57  
58  
59  
60

1  
2  
3 analyte. Simulation/measurement of mobile phase effects would improve the match between peaks  
4  
5 as well as refine estimates of  $\langle \tau_1 \rangle$  and  $\langle n \rangle$ , but lies outside the current scope of this work.  
6  
7

## 8 **5 Conclusions**

9

10  
11 Surface defects and rare chemistries can be detected and estimated using only the ensemble  
12 chromatogram. Using the DFR to translate a macroscale chromatogram in terms of microscale  
13 surface dynamics offers a route to quality by design rather than quality by testing. Mechanistic  
14 insights into the surface allow  $\theta^*$  to estimate rare retention mode prevalence with higher precision  
15 than other commonly used metrics. In absence of microscale surface measurements,  $\theta^*$  can be  
16 supplemented by  $A_s$  and skewness to refine the range of possible prevalence/relative desorption  
17 time estimates, achieving accurate measurements of surface dynamics using only macroscale data.  
18 Using the DFR, experimentally measured ensemble chromatograms can be analyzed to verify if  
19 direct observations of retention modes adequately capture qualities of the stationary phase across  
20 the whole column. The modular nature of the framework can extend our simulation to include  
21 other column effects. Future extensions could include modeling the effects of column construction  
22 such as slurry concentration, extra-column broadening effects, and patterned stationary phases.  
23 Connecting macroscale chromatograms and microscale surface dynamics directs parameter tuning  
24 using surface chemistry rather than phenomenological observations, achieving chemistry-driven  
25 design.  
26  
27  
28  
29  
30  
31  
32  
33  
34  
35  
36  
37  
38  
39  
40  
41  
42  
43  
44  
45  
46

## 47 **CRedit authorship contribution statement**

48  
49 **Logan D.C. Bishop**: Conceptualization, Methodology, Software, Formal analysis, Investigation,  
50 Writing - original draft, Writing review & editing. **Anastasiia Misiura**: Conceptualization,  
51 Methodology, Investigation, Validation, Resources, Writing - original draft. **Christy F. Landes**:  
52 Conceptualization, Methodology, Visualization, Writing - review & editing, Supervision, Project  
53 administration, Funding acquisition.  
54  
55

## 56 **Conflicts of interest**

57  
58  
59  
60

The authors declare no competing financial interest.

## Acknowledgments

C.F.L. and A.M. acknowledge the Welch Foundation (Grant C-1787) for support of this work. L.D.C.B. acknowledges that this material is based upon work supported by the National Science Foundation Graduate Research Fellowship Program (Grant 1842494).

## Author Information

Corresponding Author

\*email: [cflandes@rice.edu](mailto:cflandes@rice.edu)

## References

1. Sauer, D. G.; Melcher, M.; Mosor, M.; Walch, N.; Berkemeyer, M.; Scharl-Hirsch, T.; Leisch, F.; Jungbauer, A.; Dürauer, A., Real-time monitoring and model-based prediction of purity and quantity during a chromatographic capture of fibroblast growth factor 2. *Biotechnol. Bioeng.* **2019**, *116* (8), 1999-2009.
2. Rathore, A. S., Quality by Design (QbD)-Based Process Development for Purification of a Biotherapeutic. *Trends Biotechnol.* **2016**, *34* (5), 358-370.
3. National Academies of Science, E., and Medicine, *A Research Agenda for Transforming Separation Science*. The National Academies Press: Washington, DC, 2019.
4. Avorn, J., The \$2.6 Billion Pill - Methodologic and Policy Considerations. *New Engl. J. Med.* **2015**, *372* (20), 1877-1879.
5. Beccaria, M.; Cabooter, D., Current developments in LC-MS for pharmaceutical analysis. *Analyst* **2020**, *145* (4), 1129-1157.
6. Kiesswetter, R.; Brandl, F.; Kastner-Pustet, N.; Mannschreck, A., Chiroptical detection during liquid chromatography: Deconvolution of overlapping peaks of enantiomers and its applications. *Chirality* **2003**, *15*, S40-S49.
7. Mabry, J. N.; Skaug, M. J.; Schwartz, D. K., Single-Molecule Insights into Retention at a Reversed-Phase Chromatographic Interface. *Anal. Chem.* **2014**, *86* (19), 9451-9458.
8. Skaug, M. J.; Mabry, J. N.; Schwartz, D. K., Single-Molecule Tracking of Polymer Surface Diffusion. *J. Am. Chem. Soc.* **2014**, *136* (4), 1327-1332.
9. Wirth, M. J.; Legg, M. A., Single-molecule probing of adsorption and diffusion on silica surfaces. In *Annu. Rev. Phys. Chem.*, 2007; Vol. 58, pp 489-510.
10. Wirth, M. J.; Swinton, D. J., Single-molecule study of an adsorbed oligonucleotide undergoing both lateral diffusion and strong adsorption. *J. Phys. Chem. B* **2001**, *105* (7), 1472-1477.
11. Moringo, N. A.; Bishop, L. D. C.; Shen, H.; Misiura, A.; Carrejo, N. C.; Baiyasi, R.; Wang, W.; Ye, F.; Robinson, J. T.; Landes, C. F., A mechanistic examination of salting out in protein-polymer membrane interactions. *Proc. Natl. Acad. Sci. U.S.A.* **2019**, 201909860.
12. Kisley, L.; Chen, J. X.; Mansur, A. P.; Shuang, B.; Kourentzi, K.; Poongavanam, M. V.; Chen, W. H.; Dhamane, S.; Willson, R. C.; Landes, C. F., Unified superresolution experiments and stochastic



theory provide mechanistic insight into protein ion-exchange adsorptive separations. *Proc. Natl. Acad. Sci. U.S.A.* **2014**, *111* (6), 2075-2080.

13. Kisley, L.; Chen, J. X.; Mansur, A. P.; Dominguez-Medina, S.; Kulla, E.; Kang, M. K.; Shuang, B.; Kourentzi, K.; Poongavanam, M. V.; Dhamane, S.; Willson, R. C.; Landes, C. F., High ionic strength narrows the population of sites participating in protein ion-exchange adsorption: A single-molecule study. *J. Chromatogr. A* **2014**, *1343*, 135-142.

14. Cavazzini, A.; Dondi, F.; Jaulmes, A.; Vidal-Madjar, C.; Felinger, A., Monte Carlo model of nonlinear chromatography: correspondence between the microscopic stochastic model and the macroscopic Thomas kinetic model. *Anal. Chem.* **2002**, *74* (24), 6269-6278.

15. Dondi, F.; Munari, P.; Remelli, M.; Cavazzini, A., Monte Carlo model of nonlinear chromatography. *Anal. Chem.* **2000**, *72* (18), 4353-4362.

16. Calabrese, W.; Bishop, L. D. C.; Dutta, C.; Misiura, A.; Landes, C. F.; Kisley, L., Transforming Separation Science with Single-Molecule Methods. *Anal. Chem.* **2020**, *92* (20), 13622-13629.

17. Pamme, N., Continuous flow separations in microfluidic devices. *Lab Chip* **2007**, *7* (12), 1644.

18. Catani, M.; Ismail, O. H.; Gasparrini, F.; Antonelli, M.; Pasti, L.; Marchetti, N.; Felletti, S.; Cavazzini, A., Recent advancements and future directions of superficially porous chiral stationary phases for ultrafast high-performance enantioseparations. *Analyst* **2017**, *142* (4), 555-566.

19. Wünsch, U. J.; Hawkes, J. A., Mathematical chromatography deciphers the molecular fingerprints of dissolved organic matter. *The Analyst* **2020**, *145* (5), 1789-1800.

20. Leško, M.; Samuelsson, J.; Glenne, E.; Kaczmarski, K.; Fornstedt, T., Predictions of overloaded concentration profiles in supercritical fluid chromatography. *J. Chromatogr. A* **2021**, *1639*, 461926.

21. Vajda, P.; Guiochon, G., The modeling of overloaded elution band profiles in supercritical fluid chromatography. *J. Chromatogr. A* **2014**, *1333*, 116-123.

22. Gritti, F.; Felinger, A.; Guiochon, G., Overloaded gradient elution chromatography on heterogeneous adsorbents in reversed-phase liquid chromatography. *J. Chromatogr. A* **2003**, *1017* (1-2), 45-61.

23. Fornstedt, T.; Zhong, G. M.; Guiochon, G., Peak tailing and mass transfer kinetics in linear chromatography. *J. Chromatogr. A* **1996**, *741* (1), 1-12.

24. Felinger, A., Molecular movement in an HPLC column: A stochastic analysis. *LCGC North Am.* **2004**, *22* (7), 642-647.

25. Giddings, J. C., Kinetic Origin of Tailing in Chromatography. *Anal. Chem.* **1963**, *35* (13), 1999-&.

26. Excoffier, J. L.; Jaulmes, A.; Vidalmadjar, C.; Guiochon, G., Characterization of Small Variations in Profiles of Chromatographic Elution Peaks and Effect of Nonlinearity of Sorption Isotherm. *Anal. Chem.* **1982**, *54* (12), 1941-1947.

27. Rogers, B. A.; Wu, Z.; Wei, B. C.; Zhang, X. M.; Cao, X.; Alabi, O.; Wirth, M. J., Submicrometer Particles and Slip Flow in Liquid Chromatography. *Anal. Chem.* **2015**, *87* (5), 2520-2526.

28. Felinger, A., *Data analysis and signal processing in chromatography*. Elsevier: 1998; Vol. 21.

29. Komsta, L.; Heyden, Y.; Sherma, J., *Chemometrics in Chromatography*. CRC Press: Boca Raton, 2018.

30. Dondi, F., Approximation Properties of the Edgeworth Cramer Series and Determination of Peak Parameters of Chromatographic Peaks. *Anal. Chem.* **1982**, *54* (3), 473-477.

31. Gergely, A.; Horvath, P.; Noszal, B., Deconvolution of composite chromatographic peaks by simultaneous dual detections. *J. Chromatogr. Sci.* **2000**, *38* (10), 425-429.

32. Trapp, O., Chromatographic peak deconvolution of constitutional isomers by multiple-reaction-monitoring mass spectrometry. *J. Chromatogr. A* **2010**, *1217* (7), 1010-1016.

33. Baeza-Baeza, J. J.; Ruiz-Angel, M. J.; Garcia-Alvarez-Coque, M. C.; Carda-Broch, S., Half-width plots, a simple tool to predict peak shape, reveal column kinetics and characterise chromatographic columns in liquid chromatography: state of the art and new results. *J. Chromatogr. A* **2013**, *1314*, 142-53.

34. Wahab, M. F.; Patel, D. C.; Armstrong, D. W., Peak Shapes and Their Measurements: The Need and the Concept Behind Total Peak Shape Analysis. *LC GC Eur.* **2017**, *30* (12), 670-678.

- 1  
2  
3 35. Mockl, L.; Moerner, W. E., Super-resolution Microscopy with Single Molecules in Biology and  
4 Beyond-Essentials, Current Trends, and Future Challenges. *J. Am. Chem. Soc.* **2020**, *142* (42), 17828-  
5 17844.
- 6 36. Chen, H. H.; Xie, X. H.; Chen, T. Y., Single-molecule microscopy for in-cell quantification of  
7 protein oligomeric stoichiometry. *Curr. Opin. Struct. Biol.* **2021**, *66*, 112-118.
- 8 37. Pan, M.; Zhang, Y.; Yan, G.; Chen, T.-Y., Dissection of Interaction Kinetics through Single-  
9 Molecule Interaction Simulation. *Anal. Chem.* **2020**, *92* (17), 11582-11589.
- 10 38. Bishop, L. D. C.; Misiura, A.; Moringo, N. A.; Landes, C. F., Unraveling peak asymmetry in  
11 chromatography through stochastic theory powered Monte Carlo simulations. *J. Chromatogr. A* **2020**,  
12 *1625*, 461323.
- 13 39. Rix, H., Detection of Small Variations in Shape Between Two Chromatographic Peaks. *J.*  
14 *Chromatogr.* **1981**, *204* (JAN), 163-165.
- 15 40. Rix, H.; Malenge, J. P., Detecting Small Variations in Shape. *IEEE Trans. Syst. Man Cybern.*  
16 **1980**, *10* (2), 90-96.
- 17 41. Roles, J.; Guiochon, G., Precision and accuracy of the gas solid adsorption-isotherms derived by  
18 the elution-by-characteristic-points method. *J. Chromatogr.* **1992**, *591* (1-2), 245-265.
- 19 42. Pasti, L.; Cavazzini, A.; Felinger, A.; Martin, M.; Dondi, F., Single-molecule observation and  
20 chromatography unified by levy process representation. *Anal. Chem.* **2005**, *77* (8), 2524-2535.
- 21 43. Moringo, N. A.; Bishop, L. D. C.; Shen, H.; Misiura, A.; Carrejo, N. C.; Baiyasi, R.; Wang, W.;  
22 Ye, F.; Robinson, J. T.; Landes, C. F., A mechanistic examination of salting out in protein-polymer  
23 membrane interactions. *Proceedings of the National Academy of Sciences* **2019**, *116* (46), 22938-22945.
- 24 44. Jensen, K. H.; Valente, A.; Stone, H. A., Flow rate through microfilters: Influence of the pore size  
25 distribution, hydrodynamic interactions, wall slip, and inertia. *Phys. Fluids* **2014**, *26* (5), 13.
- 26 45. Wu, Z.; Wei, B. C.; Zhang, X. M.; Wirth, M. J., Efficient Separations of Intact Proteins Using  
27 Slip-Flow with Nano-Liquid Chromatography-Mass Spectrometry. *Anal. Chem.* **2014**, *86* (3), 1592-1598.
- 28 46. Vanson, J. M.; Boutin, A.; Klotz, M.; Coudert, F. X., Transport and adsorption under liquid flow:  
29 the role of pore geometry. *Soft Matter* **2017**, *13* (4), 875-885.
- 30 47. Gritti, F.; Hochstrasser, J.; Svidrytski, A.; Hlushkou, D.; Tallarek, U., Morphology-transport  
31 relationships in liquid chromatography: Application to method development in size exclusion  
32 chromatography. *J. Chromatogr. A* **2020**, *1620*, 16.
- 33 48. Salmean, C.; Dimartino, S., 3D-Printed Stationary Phases with Ordered Morphology: State of the  
34 Art and Future Development in Liquid Chromatography. *Chromatographia* **2019**, *82* (1), 443-463.
- 35 49. Tallarek, U.; Hlushkou, D.; Rybka, J.; Holtzel, A., Multiscale Simulation of Diffusion in Porous  
36 Media: From Interfacial Dynamics to Hierarchical Porosity. *J. Phys. Chem. C* **2019**, *123* (24), 15099-  
37 15112.
- 38 50. Tallarek, U.; Hochstrasser, J.; Ziegler, F.; Huang, X. H.; Kubel, C.; Buchmeiser, M. R., Olefin  
39 Ring-closing Metathesis under Spatial Confinement: Morphology-transport Relationships. *ChemCatChem*  
40 **2021**, *13* (1), 281-292.
- 41 51. Vanderheyden, Y.; Vanderlinden, K.; Broeckhoven, K.; Desmet, G., Problems involving the  
42 determination of the column-only band broadening in columns producing narrow and tailed peaks. *J.*  
43 *Chromatogr. A* **2016**, *1440*, 74-84.
- 44 52. Gritti, F.; Brousmiche, D.; Gilar, M.; Water, T. H.; Wyndham, K., Kinetic mechanism of water  
45 dewetting from hydrophobic stationary phases utilized in liquid chromatography. *J. Chromatogr. A* **2019**,  
46 *1596*, 41-53.
- 47 53. Grabarics, M.; Lettow, M.; Kirk, A. T.; Von Helden, G.; Causon, T. J.; Pagel, K., Plate-height  
48 model of ion mobility-mass spectrometry. *Analyst* **2020**, *145* (19), 6313-6333.
- 49 54. Kumarasinghe, R.; Ito, T.; Higgins, D. A., Nanoconfinement and Mass Transport in Silica  
50 Mesopores: the Role of Charge at the Single Molecule and Single Pore Levels. *Anal. Chem.* **2020**, *92* (1),  
51 1416-1423.  
52  
53  
54  
55  
56  
57  
58  
59  
60

- 1  
2  
3 55. Ghimire, G.; Espinoza, R.; Xu, H.; Nasaka, S.; Kameta, N.; Masuda, M.; Higgins, D. A.; Ito, T.,  
4 Diffusion Behavior of Differently Charged Molecules in Self-Assembled Organic Nanotubes Studied  
5 Using Imaging Fluorescence Correlation Spectroscopy. *Langmuir* **2019**, *35* (24), 7783-7790.
- 6 56. Xu, H.; Nagasaka, S.; Kameta, N.; Masuda, M.; Ito, T.; Higgins, D. A., Spectroscopic imaging  
7 studies of nanoscale polarity and mass transport phenomena in self-assembled organic nanotubes. *PCCP*  
8 **2017**, *19* (30), 20040-20048.
- 9 57. Rybka, J.; Hölzel, A.; Steinhoff, A.; Tallarek, U., Molecular Dynamics Study of the Relation  
10 between Analyte Retention and Surface Diffusion in Reversed-Phase Liquid Chromatography. *The*  
11 *Journal of Physical Chemistry C* **2019**.
- 12 58. Bishop, L. D. C.; Landes, C. F., From a Protein's Perspective: Elution at the Single-Molecule  
13 Level. *Acc. Chem. Res.* **2018**, *51* (9), 2247-2254.
- 14 59. Moringo, N. A.; Shen, H.; Bishop, L. D. C.; Wang, W.; Landes, C. F., Enhancing Analytical  
15 Separations Using Super-Resolution Microscopy. *Annu. Rev. Phys. Chem.* **2018**, *69* (1), 353-375.
- 16 60. Liu, H. B.; Jeong, J.; Kao, Y. H.; Zhang, Y. T., Characterization of free thiol variants of an IgG1  
17 by reversed phase ultra high pressure liquid chromatography coupled with mass spectrometry. *J. Pharm.*  
18 *Biomed. Anal.* **2015**, *109*, 142-149.
- 19 61. Cavazzini, A.; Remelli, M.; Dondi, F., Stochastic theory of two-site adsorption chromatography  
20 by the characteristic function method. *J. Microcolumn Sep.* **1997**, *9* (4), 295-302.
- 21 62. Felinger, A., Determination of rate constants for heterogeneous mass transfer kinetics in liquid  
22 chromatography. *J. Chromatogr. A* **2006**, *1126* (1-2), 120-128.
- 23 63. Giddings, J. C., Kinetic Model for Chromatographic Dispersion and Electrodiffusion. *J. Chem.*  
24 *Phys.* **1957**, *26* (6), 1755-1756.
- 25 64. Giddings, J. C., Stochastic Considerations on Chromatographic Dispersion. *J. Chem. Phys.* **1957**,  
26 *26* (1), 169-173.
- 27 65. Kumar, K. V.; Gadipelli, S.; Wood, B.; Ramisetty, K. A.; Stewart, A. A.; Howard, C. A.; Brett,  
28 D. J. L.; Rodriguez-Reinoso, F., Characterization of the adsorption site energies and heterogeneous  
29 surfaces of porous materials. *J. Mater. Chem. A* **2019**, *7* (17), 10104-10137.
- 30 66. Wirth, M. J.; Swinton, D. J., Single-molecule probing of mixed-mode adsorption at a  
31 chromatographic interface. *Anal. Chem.* **1998**, *70* (24), 5264-5271.
- 32 67. Kisley, L.; Patil, U.; Dhamane, S.; Kourentzi, K.; Tauzin, L. J.; Willson, R. C.; Landes, C. F.,  
33 Competitive multicomponent anion exchange adsorption of proteins at the single molecule level. *Analyst*  
34 **2017**, *142* (17), 3127-3131.
- 35 68. Zhou, J. J.; Wang, M. Q.; Zhang, B. L.; Zhang, Q. Y., Metal coordination assisted thermo-  
36 sensitive magnetic imprinted microspheres for selective adsorption and efficient elution of proteins.  
37 *Colloid Surf. A-Physicochem. Eng. Asp.* **2021**, *612*, 9.
- 38 69. Giddings, J. C.; Eyring, H., A Molecular Dynamic Theory of Chromatography. *J. Phys. Chem.*  
39 **1955**, *59* (5), 416-421.
- 40 70. Mcquarrie, D. A., On Stochastic Theory of Chromatography. *J. Chem. Phys.* **1963**, *38* (2), 437-  
41 445.
- 42 71. Felinger, A.; Pasti, L.; Dondi, F., Fourier-Analysis of Multicomponent Chromatograms - Theory  
43 and Models. *Anal. Chem.* **1990**, *62* (17), 1846-1853.
- 44 72. Desmet, G., A finite parallel zone model to interpret and extend Giddings' coupling theory for the  
45 eddy-dispersion in porous chromatographic media. *J. Chromatogr. A* **2013**, *1314*, 124-137.
- 46 73. Wirth, M. J.; Ludes, M. D.; Swinton, D. J., Spectroscopic observation of adsorption to active  
47 silanols. *Anal. Chem.* **1999**, *71* (18), 3911-3917.
- 48 74. Dondi, F.; Cavazzini, A.; Martin, M., Correspondence between chromatography, single-molecule  
49 dynamics, and equilibrium: A stochastic approach. In *Advances in Chromatography, Vol 43*, Brown, P.  
50 R.; Grushka, E.; Lunte, S., Eds. Marcel Dekker: New York, 2005; Vol. 43, pp 179-230.
- 51 75. Dondi, F.; Guiochon, G., *Theoretical Advancement in Chromatography and Related Separation*  
52 *Techniques*. 1 ed.; Springer Netherlands: 1992.
- 53  
54  
55  
56  
57  
58  
59  
60

- 1  
2  
3 76. McLachlan, G. J.; Lee, S. X.; Rathnayake, S. I., Finite Mixture Models. *Annual Review of*  
4 *Statistics and Its Application* **2019**, *6* (1), 355-378.
- 5 77. Hlushkou, D.; Svidrytski, A.; Tallarek, U., Tracer-Size-Dependent Pore Space Accessibility and  
6 Long-Time Diffusion Coefficient in Amorphous, Mesoporous Silica. *J. Phys. Chem. C* **2017**, *121* (15),  
7 8416-8426.
- 8 78. Schweiger, S.; Hinterberger, S.; Jungbauer, A., Column-to-column packing variation of  
9 disposable pre-packed columns for protein chromatography. *J. Chromatogr. A* **2017**, *1527*, 70-79.
- 10 79. Desmet, G.; Broeckhoven, K., Extra-column band broadening effects in contemporary liquid  
11 chromatography: Causes and solutions. *Trac-Trends Anal. Chem.* **2019**, *119*, 14.
- 12 80. Reising, A. E.; Schlabach, S.; Baranau, V.; Stoeckel, D.; Tallarek, U., Analysis of packing  
13 microstructure and wall effects in a narrow-bore ultrahigh pressure liquid chromatography column using  
14 focused ion-beam scanning electron microscopy. *J. Chromatogr. A* **2017**, *1513*, 172-182.
- 15 81. Dondi, F.; Remelli, M., The characteristic function method in the stochastic theory of  
16 chromatography. *J. Phys. Chem.* **1986**, *90* (9), 1885-1891.
- 17 82. Papai, Z.; Pap, T. L., Analysis of peak asymmetry in chromatography. *J. Chromatogr. A* **2002**,  
18 *953* (1-2), 31-38.
- 19 83. Wahab, M. F.; Patel, D. C.; Armstrong, D. W., Total peak shape analysis: detection and  
20 quantitation of concurrent fronting, tailing, and their effect on asymmetry measurements. *J. Chromatogr.*  
21 *A* **2017**, *1509*, 163-170.
- 22 84. Wahab, M. F.; O'Haver, T. C.; Gritti, F.; Hellinghausen, G.; Armstrong, D. W., Increasing  
23 chromatographic resolution of analytical signals using derivative enhancement approach. *Talanta* **2019**,  
24 *192*, 492-499.
- 25 85. Millman, K. J.; Aivazis, M., Python for Scientists and Engineers. *Comput. Sci. Eng.* **2011**, *13* (2),  
26 9-12.
- 27 86. van der Walt, S.; Colbert, S. C.; Varoquaux, G., The NumPy Array: A Structure for Efficient  
28 Numerical Computation. *Comput. Sci. Eng.* **2011**, *13* (2), 22-30.
- 29 87. Virtanen, P.; Gommers, R.; Oliphant, T. E.; Haberland, M.; Reddy, T.; Cournapeau, D.;  
30 Burovski, E.; Peterson, P.; Weckesser, W.; Bright, J.; van der Walt, S. J.; Brett, M.; Wilson, J.; Millman,  
31 K. J.; Mayorov, N.; Nelson, A. R. J.; Jones, E.; Kern, R.; Larson, E.; Carey, C. J.; Polat, I.; Feng, Y.;  
32 Moore, E. W.; VanderPlas, J.; Laxalde, D.; Perktold, J.; Cimrman, R.; Henriksen, I.; Quintero, E. A.;  
33 Harris, C. R.; Archibald, A. M.; Ribeiro, A. N. H.; Pedregosa, F.; van Mulbregt, P.; SciPy, C., SciPy 1.0:  
34 fundamental algorithms for scientific computing in Python. *Nat. Methods* **2020**, *17* (3), 261-272.
- 35 88. Felinger, A.; Pasti, L.; Dondi, F.; van Hulst, M.; Schoenmakers, P. J.; Martin, M., Stochastic  
36 theory of size exclusion chromatography: Peak shape analysis on single columns. *Anal. Chem.* **2005**, *77*  
37 (10), 3138-3148.
- 38 89. Felinger, A., Molecular dynamic theories in chromatography. *J. Chromatogr. A* **2008**, *1184* (1-2),  
39 20-41.
- 40 90. Hlushkou, D.; Gritti, F.; Daneyko, A.; Guiochon, G.; Tallarek, U., How Microscopic  
41 Characteristics of the Adsorption Kinetics Impact Macroscale Transport in Chromatographic Beds. *J.*  
42 *Phys. Chem. C* **2013**, *117* (44), 22974-22985.
- 43 91. Hlushkou, D.; Gritti, F.; Guiochon, G.; Seidel-Morgenstern, A.; Tallarek, U., Effect of  
44 Adsorption on Solute Dispersion: A Microscopic Stochastic Approach. *Anal. Chem.* **2014**, *86* (9), 4463-  
45 4470.
- 46 92. Horvath, K.; Olajos, M.; Felinger, A.; Hajos, P., Retention controlling and peak shape simulation  
47 in anion chromatography using multiple equilibrium model and stochastic theory. *J. Chromatogr. A* **2008**,  
48 *1189* (1-2), 42-51.
- 49 93. Cavazzini, A.; Remelli, M.; Dondi, F.; Felinger, A., Stochastic theory of multiple-site linear  
50 adsorption chromatography. *Anal. Chem.* **1999**, *71* (16), 3453-3462.
- 51 94. Savitzky, A.; Golay, M. J. E., Smoothing + differentiation of data by simplified least squares  
52 procedures. *Anal. Chem.* **1964**, *36* (8), 1627-1639.
- 53  
54  
55  
56  
57  
58  
59  
60

- 1  
2  
3 95. Lytle, F. E.; Julian, R. K., Automatic Processing of Chromatograms in a High-Throughput  
4 Environment. *Clin. Chem.* **2016**, *62* (1), 144-153.
- 5 96. Broeckhoven, K.; Eeltink, S.; De Malsche, W.; Matheuse, F.; Desmet, G.; Cabooter, D., Current  
6 and Future Chromatographic Columns: Is One Column Enough to Rule Them All? *LCGC North Am.*  
7 **2018**, *36* (6), 9-17.
- 8 97. Desmet, G.; Cabooter, D.; Broeckhoven, K., Graphical Data Representation Methods To Assess  
9 the Quality of LC Columns. *Anal. Chem.* **2015**, *87* (17), 8593-8602.
- 10 98. Kadjo, A. F.; Dasgupta, P. K.; Srinivasan, K., Shape-Based Peak Identity Confirmation in Liquid  
11 Chromatography. *Anal. Chem.* **2021**, *93* (8), 3848-3856.
- 12 99. Cooper, J. T.; Harris, J. M., Imaging Fluorescence-Correlation Spectroscopy for Measuring Fast  
13 Surface Diffusion at Liquid/Solid Interfaces. *Anal. Chem.* **2014**, *86* (15), 7618-7626.
- 14 100. Cooper, J. T.; Peterson, E. M.; Harris, J. M., Fluorescence Imaging of Single-Molecule Retention  
15 Trajectories in Reversed-Phase Chromatographic Particles. *Anal. Chem.* **2013**, *85* (19), 9363-9370.
- 16 101. Moringo, N. A.; Shen, H.; Tauzin, L. J.; Wang, W. X.; Bishop, L. D. C.; Landes, C. F., Variable  
17 Lysozyme Transport Dynamics on Oxidatively Functionalized Polystyrene Films. *Langmuir* **2017**, *33*  
18 (41), 10818-10828.
- 19 102. Hansen, J.; Ely, K.; Horsley, D.; Herron, J.; Hlady, V.; Andrade, J. D., The adsorption of  
20 lysozymes: A model system. *Makromolekulare Chemie. Macromolecular Symposia* **1988**, *17* (1), 135-  
21 154.  
22  
23  
24  
25  
26  
27  
28  
29  
30  
31  
32  
33  
34  
35  
36  
37  
38  
39  
40  
41  
42  
43  
44  
45  
46  
47  
48  
49  
50  
51  
52  
53  
54  
55  
56  
57  
58  
59  
60